Analytical Modeling of Manufacturing Tolerances for Surface Mounted Permanent Magnet Synchronous Machines

Michael Schröder, David Franck, and Kay Hameyer, *Senior Member, IEEE*

***Abstract*—No production process of electrical machines is ideal. During the process, various stochastic manufacturing deviations can occur. Common tolerances are for example static or dynamic rotor eccentricities, asymmetric stator teeth if segmented sheets are used or – for electrical machines with permanent magnets (PMs) – a variable magnetic behavior caused by material or due to the magnetization process. Manufacturing tolerances can affect the acoustic emission of an electrical machine significantly. To estimate the influence of tolerances in an early design stage of an electrical machine, an analytical approach based on conformal mapping (CM) is presented here to model manufacturing tolerances for surface mounted permanent magnet synchronous machines (PMSMs) and calculate the tolerances' impact on radial force densities in an acceptable computational time.**

***Index Terms*—Acoustic emission, analytical models, electromagnetic analysis, electromagnetic fields, electromagnetic forces, magnetic flux density, magnetization, manufacturing, permanent magnet machines, permeability, tolerance analysis.**

I. Introduction

THE conformal mapping approach dates back to the beginning of the 20th century, where Carter presented the analytical calculation of the magnetic air gap field in electrical machines, e. g. in [1]. 80 years later, Žarko et al. presented a complex-valued spatial varying permeance function to describe the influence of slotting in radial and tangential direction [2]. Assumptions made for this approach are ideal ferromagnetic material properties in stator and rotor (relative magnetic permeability $\mu_\mathrm{r} \to \infty$) and linear material properties in the air and in the permanent magnets ($\mu_\mathrm{r} = \text{const.}$). As described by Hafner et al. in [3], the CM approach allows the calculation of the air gap's magnetic field $\underline{B}_\mathrm{Airgap}(\alpha, t)$ out of its main contributing components:

$$\underline{B}_\mathrm{Airgap}(\alpha, t) = \underline{B}_\mathrm{PM}(\alpha, t) \cdot \underline{\lambda}^*(\alpha) + \underline{B}_\mathrm{Stator}(\alpha, t) \ , \qquad (1)$$

where $\underline{B}_\mathrm{PM}(\alpha, t)$ describes the magnetic air gap field of the rotor created by the PMs, in dependence of the coordinate angle $\alpha \in [0, 2\pi)$ and time t, under the assumption of an unslotted, infinite permeable stator. The stator's magnetic air gap field created by the current conducting coils is considered by the component $\underline{B}_\mathrm{Stator}(\alpha, t)$ and the influence of the stator's slotting onto the rotor's unslotted magnetic field is described by the relative permeance function $\underline{\lambda}(\alpha)$. $\underline{\lambda}^*(\alpha)$ is the conjugate-complex value of the relative permeance function. Those three contributing components are all complex-valued quantities, where the real value represents the radial component and the imaginary value represents the tangential component – e. g. for the rotor's magnetic field:

$$\underline{B}_\mathrm{PM}(\alpha, t) = B_\mathrm{PM,\,rad}(\alpha, t) + \mathrm{j} \cdot B_\mathrm{PM,\,tan}(\alpha, t) \ . \qquad (2)$$

The force density $\underline{\sigma}(\alpha, t)$ acting on a surface can generally be calculated out of the complex magnetic field $\underline{B}(\alpha, t)$ in the surrounding air:

$$\underline{\sigma}(\alpha, t) = \frac{\underline{B}^2(\alpha, t)}{2\mu_0} \ . \qquad (3)$$

This equation can be derived from the Lorentz force and can be simplified by means of the Maxwell stress tensor. μ_0 is the permeability of free space. For cylindrical objects, such as the rotor of an electrical machine, (3) can be split up in a real-valued radial force density component

$$\sigma_\mathrm{rad}(\alpha, t) = \frac{1}{2\mu_0} \cdot \left(B_\mathrm{rad}^2(\alpha, t) - B_\mathrm{tan}^2(\alpha, t)\right) \qquad (4)$$

$$\approx \frac{1}{2\mu_0} \cdot B_\mathrm{rad}^2(\alpha, t) \qquad (5)$$

and an imaginary tangential force density component

$$\sigma_\mathrm{tan}(\alpha, t) = \frac{1}{\mu_0} \cdot B_\mathrm{rad}(\alpha, t) \cdot B_\mathrm{tan}(\alpha, t) \ . \qquad (6)$$

The relative magnetic permeability μ_r of the ferromagnetic material in an electrical machine is much higher than in the air gap (e. g. $\mu_\mathrm{r,\,Fe} \approx 10\,000 \gg \mu_\mathrm{r,\,Air} \approx 1$). For this reason, the magnetic flux lines run predominantly in radial direction through the machine's air gap, so that the radial flux density $B_\mathrm{rad}(\alpha, t)$ is much higher than the tangential one $B_\mathrm{tan}(\alpha, t)$. This results in the simplified approximation (5) which is often used in literature, if just the radial flux density is calculated analytical and the tangential flux density is not calculated. In [4], Wu et al. show a model which is based on an analytical field model for the slotless fractional-slot PM machine and accounts for the influence of both the radial and tangential force components under any load condition.

The tangential force density $\sigma_\mathrm{tan}(\alpha, t)$ is necessary for the torque production in the electrical machine. The integral over

M. Schröder is with the Institute of Electrical Machines, RWTH Aachen University, Schinkelstraße 4, D-52056 Aachen, Germany (corresponding author; phone: +49 241 80 97667; fax: +49 241 80 92270; e-mail: michael.schroeder@iem.rwth-aachen.de).

D. Franck is with the Institute of Electrical Machines, RWTH Aachen University, Schinkelstraße 4, D-52056 Aachen, Germany (e-mail: david.franck@iem.rwth-aachen.de).

K. Hameyer is with the Institute of Electrical Machines, RWTH Aachen University, Schinkelstraße 4, D-52056 Aachen, Germany (e-mail: kay.hameyer@iem.rwth-aachen.de).

978-1-4799-7941-7/15/$31.00 ©2015 IEEE

the tangential force density along the air gap in circumferential direction yields the mechanical torque

$$M(t) = r \cdot F_{\text{tan}}(t) = r^2 \cdot l \cdot \int_0^{2\pi} \sigma_{\text{tan}}(\alpha, t)\, \mathrm{d}\alpha\,, \qquad (7)$$

where r is the radius, $F_{\text{tan}}(t)$ the sum force in tangential direction and l the length of a visualized cylinder in the machine's air gap.

The major radial force density $\sigma_{\text{rad}}(\alpha, t)$ otherwise acts on the stator teeth. It deforms the stator and is so essentially the reason for sound radiation. Due to Newton's third law, the radial forces act also on the rotor and especially on the rotor's bearing. The integral over the radial force density results in the sum force $F_{\text{rad}}(t)$ in radial direction – the so called unbalanced magnetic pull (UMP) [5]

$$F_{\text{rad}}(t) = r \cdot l \cdot \int_0^{2\pi} \sigma_{\text{rad}}(\alpha, t)\, \mathrm{d}\alpha\,, \qquad (8)$$

a sum force between the stator and rotor of an electrical machine resulting from a difference in the air gap flux densities on opposite sides of the machine. This difference in flux density is, in general, caused by a difference in the air gaps on the two sides [6], e. g. due to rotor eccentricity. Especially crucial for the bearings are revolving radial forces, which are described by the alternating component of the radial force.

A practice similar to the conformal mapping approach is described by Zhu et al. in [7] with the so called field reconstruction (FR) method. With this method, radial and tangential force components can be calculated fast during the engineering process of an electrical machine for various stator current excitations. For that purpose, the magnetic field of the PMs and the field induced by a current conducting conductor in one slot are calculated separately via finite element analysis (FEA) just once. The so computed single fields are reconstructed subsequent to the whole magnetic air gap field in dependence of rotor position, winding layout and current feed. This procedure needs less calculation time than a full FEA for every time step.

A related manner is presented by Hafner et al. in [8]. An extension of the classical CM approach is presented there. Additional CM parameters are computed from single finite element (FE) computations, so that effects like slot leakage or saturation can be considered in the model over a wide operation range of the electrical machine.

Both approaches provide an accuracy similar to that of FE simulations with however the low computation time that is characteristic for analytical models.

In this paper the classical analytical CM approach is used and expanded to model the influence of manufacturing tolerances. It can be assumed that the presented approach can also be applied, if the CM functions are determined by means of FE simulations like in [7] or [8].

II. Modeling of Manufacturing Tolerances

This section describes the modeling of different manufacturing tolerances and how they influence the relative permeance function, the magnetic air gap field of the rotor created by the PMs and the stator's magnetic air gap field created by the current conducting coils. The manufacturing tolerances have to be considered in all of the three contributing components.

A. Relative Permeance Function

The relative permeance function $\underline{\lambda}(\alpha)$ is an unit-less quantity, which describes the ratio of the flux density in the slotted air gap to the flux density in the unslotted air gap [2]. For a machine with an ideal stator without manufacturing tolerances, a relative permeance function is calculated once for one slot pitch and is than replicated for every slot pitch in the entire air gap to receive the complete permeance function, as it is described in [2]. The only parameters needed for the calculation are the outer rotor radius, the heights of the magnets and the air gap, the length of a slot pitch and the slot opening factor.

If the stator is not ideal and the slot width changes from one slot pitch to the other, for example due to asymmetrical stator teeth if segmented sheets are used, a relative permeance function $\underline{\lambda}_i$ has to be calculated for every different slot pitch i and then concatenated to the entire permeance function:

$$\underline{\lambda}(\alpha) = \sum_{i=0}^{N_1-1} \underline{\lambda}_i \left(\alpha - \sum_{j=0}^{i} \tau_{\text{S},\,j} \right)\,, \qquad (9)$$

where N_1 is equal to the number of slot pitches and $\tau_{\text{S},\,j}$ is the width of the j-th slot pitch, measured at the radius r.

The described approach is to be presented for a six teeth ($N_1 = 6$) and four poles ($2p = 4$) surface mounted permanent magnet synchronous machine. The geometrical, material and rating data of the exemplary investigated machine are presented in Table I. It can be noted, that the presented approach is also valid for other surface mounted PMSMs.

Fig. 1 shows a calculated permeance function in radial direction for the described surface mounted PMSM and Fig. 2 the corresponding function in tangential direction. For the calculation, the third tooth is displaced by $8°$. This value is chosen, so that the effect on the permeance function is clearly visible. In practice, the value for tooth displacement is smaller. In order to represent the tooth displacement with help of the CM approach, the width of the second slot and slot

TABLE I
Electrical Machine's Geometrical, Material and Rating Data

Parameter	Value	Parameter	Value
Rating Speed	3000 min^{-1}	Shaft Diameter	9 mm
Rating Current	2.3 A	Bore Diameter	40 mm
Rating Torque	2 Nm	Outer Diameter	130 mm
Phases	3	Stator Yoke Height	15 mm
Pole Pairs	2	Tooth Width	10 mm
Stator Slots	6	Air Gap Height	2 mm
Number of Turns	90	PM Height	3 mm
Copper Space Factor	47 %	Rotor Slot Depth	1 mm
Rem. Flux Density	1.04 T	Active Length	120 mm
Rel. PM Permeability	1.05	Pole Pitch Factor	82.5 %

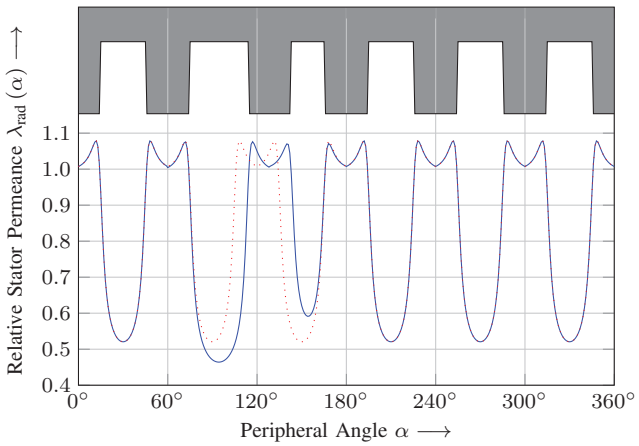

Fig. 1. Relative radial permeance function for a stator with six teeth, where the third tooth is displaced (solid) and for the ideal stator (dotted). A schematic of the tolerance afflicted stator is shown above the course of the function.

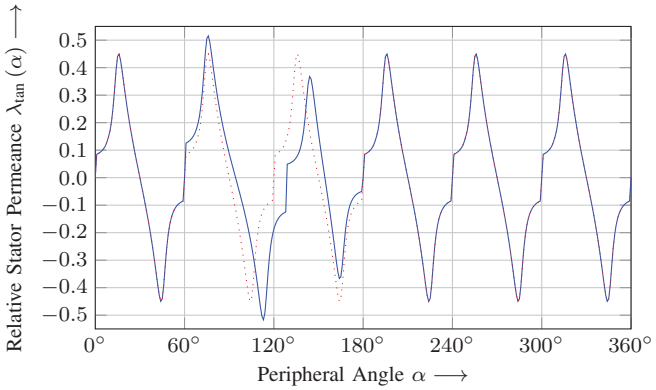

Fig. 2. Relative tangential permeance function for a stator with six teeth, where the third tooth is displaced (solid) and for the ideal stator (dotted).

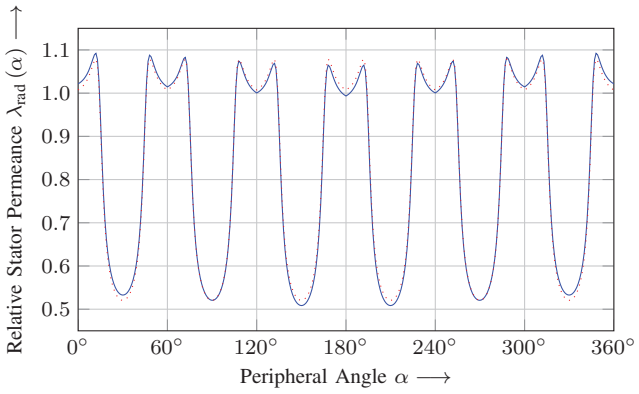

Fig. 3. Relative radial permeance function for a six teeth and four poles surface mounted PMSM with a static eccentricity of 0.5 mm (solid) and for the ideal machine (dotted).

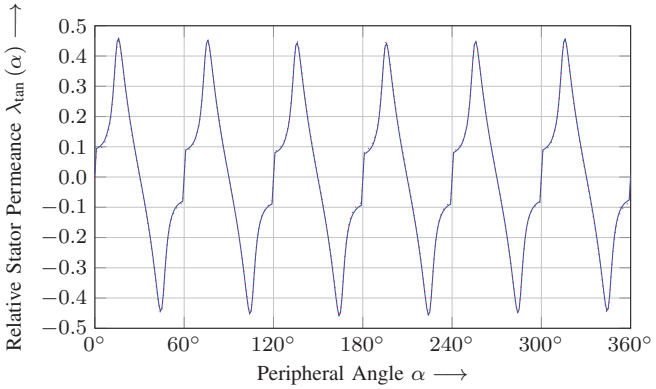

Fig. 4. Relative tangential permeance function for a six teeth and four poles surface mounted PMSM with a static eccentricity of 0.5 mm (solid) and for the ideal machine (dotted).

pitch increases and the width of the third slot and slot pitch decreases. For comparison, the symmetric permeance function of the ideal stator without manufacturing tolerances is drawn dotted in the figures. A schematic of the tolerance afflicted stator is shown above the course of the function in Fig. 1.

If there is a static rotor eccentricity, the permeance function is superposed by a sinusoid [9]. With help of the conformal mapping approach, the permeance function is calculated once for the smallest air gap δ_{min} and once for the largest air gap δ_{max}. Then the permeance function $\underline{\lambda}_{\text{ecc, stat}}(\alpha)$, afflicted with a static eccentricity, is computed sinusoidal between the permeance functions for the smallest and largest air gap:

$$\underline{\lambda}_{\text{ecc, stat}}(\alpha) = \frac{\hat{\underline{\lambda}}_{\text{min}} - \hat{\underline{\lambda}}_{\text{max}}}{\delta_{\text{max}} - \delta_{\text{min}}} \cdot e \cdot \cos(\alpha - \varphi) + \underline{\lambda}(\alpha) \ , \quad (10)$$

where $\hat{\underline{\lambda}}_{\text{max}}$ is the maximum of the permeance functions in radial and tangential direction for the largest air gap, $\hat{\underline{\lambda}}_{\text{min}}$ the maximum of the permeance functions for the smallest air gap, e the eccentricity and φ the angle of the eccentricity, which is similar to the notation used in [5].

Fig. 3 shows a so calculated stator permeance function in radial direction for the six teeth and four poles surface mounted PMSM with a static eccentricity of 0.5 mm and an eccentricity angle $\varphi = 0$. On that account, the relative permeance increases around $0°$ and decreases at the opposite site at $180°$. The overlaid sinusoidal function is clearly identifiable. For comparison, the symmetric permeance function of the ideal machine is drawn dotted.

As expected, the same eccentricity has not much influence on the relative permeance's tangential component, as shown in Fig. 4, where the computed permeance function in tangential direction is depicted. The difference to the dotted function of the ideal machine is comparatively small.

For dynamic rotor eccentricities, the spot of the smallest air gap rotates with rotor speed along the machine's circumference. For that reason, the permeance function $\underline{\lambda}_{\text{ecc, dyn}}(\alpha, t)$, afflicted with a dynamic rotor eccentricity, becomes time-dependent, changes in every time step of the simulation and (10) turns to:

$$\underline{\lambda}_{\text{ecc, dyn}}(\alpha, t) = \frac{\hat{\underline{\lambda}}_{\text{min}} - \hat{\underline{\lambda}}_{\text{max}}}{\delta_{\text{max}} - \delta_{\text{min}}} \cdot e \cdot \cos(\alpha - \omega t - \varphi) + \underline{\lambda}(\alpha) \ , \quad (11)$$

where ω is the angular frequency of the rotor.

In general, both types of eccentricity may occur at the same time and lead to a mixed eccentricity. Because of the CM model's linearity, both types of eccentricity can be considered at the same time by superposition. Similarly, all three of the so

far presented manufacturing tolerances can be superimposed at the same time in the model.

B. Rotor Flux Density

As described by Hafner et al. in [3], there exist many possibilities for the analytical calculation of the magnetic field distribution in the air gap of PMSMs for a slotless stator. For example, the rotor flux density can be calculated for internal and external rotors, radial and parallel or radial sine and sinusoidal direction magnetizations. For the model presented in this paper, the calculation of radial magnetized magnets is implemented. Parameters needed for the calculation are the outer rotor radius, the height of the magnets and the air gap, the remanence induction and the relative permeability of the magnets, the number of poles as well as the pole pitch factor.

If the rotor is not ideal and the parameters change from one pole pitch to the other, for example if the width, the height or the remanence induction of the magnets change because of the magnet's manufacturing tolerances, a rotor flux density $\underline{B}_{\mathrm{PM},\,i}$ has to be calculated for every different pole pitch i and then concatenated to the entire rotor flux density:

$$\underline{B}'_{\mathrm{PM}}\left(\alpha, t\right) = \sum_{i=0}^{2p-1} \underline{B}_{\mathrm{PM},\,i} \left(\alpha - \sum_{j=0}^{i} \tau_{\mathrm{P},\,j} \right) , \qquad (12)$$

where $2p$ is equal to the number of poles and $\tau_{\mathrm{P},\,j}$ is the width of the j-th pole pitch.

Due to Maxwell's equations, the magnetic field $\underline{B}\left(\alpha, t\right)$ is solenoidal, i. e. the magnetic field is a divergence free vector field: $\nabla \cdot \underline{B}\left(\alpha, t\right) = 0$. For this reason, the potentially non solenoidal rotor flux density $\underline{B}'_{\mathrm{PM}}\left(\alpha, t\right)$ from (12) has to be adjusted by a correction term for every time step, which yields the tolerance afflicted rotor flux density:

$$\underline{B}_{\mathrm{PM}}\left(\alpha, t\right) = \underline{B}'_{\mathrm{PM}}\left(\alpha, t\right) - \frac{1}{2\pi} \int_{0}^{2\pi} \mathrm{Re}\left\{\underline{B}'_{\mathrm{PM}}\left(\alpha, t\right)\right\} \,\mathrm{d}\alpha\,. \qquad (13)$$

In other words, the mean value of the rotor flux density's radial component must be zero.

The effect of a smaller magnet on the radial rotor flux density for the investigated PMSM is presented in Fig. 5 and in Fig. 6 for the corresponding tangential component. The pole pitch factor of the second pole pitch around 90° is reduced by 15 %. This is equal to a magnet reduced in width, e. g. due to manufacturing variations. This value is chosen, so that the effect is clearly visible. In practice, the tolerance value is smaller. For comparison, the rotor flux density of the ideal machine is drawn dotted in the two figures. A schematic of the tolerance afflicted rotor is shown below the course of the function in Fig. 5. The smaller magnet is good recognizable in both components. The effect of the correction term (13) is visible in the radial component, where the tolerance afflicted rotor flux density has a small negative offset.

To validate the CM approach, a FE simulation is performed. The rotor of a surface mounted PMSM with the same data as presented in Table I and a 15 % smaller magnet for the second pole pitch is modeled. The stator is replaced by a

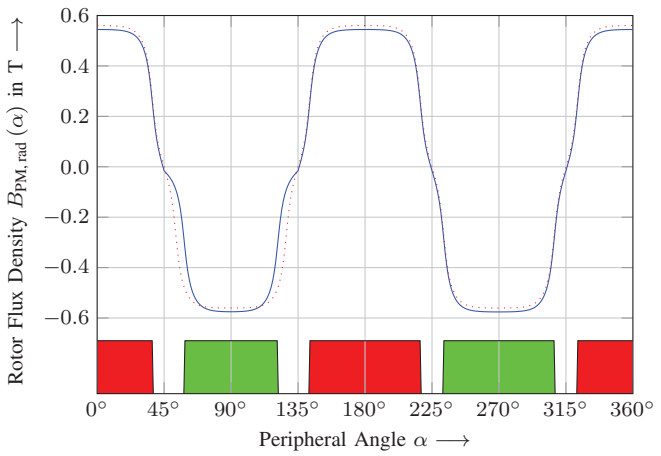

Fig. 5. Radial rotor flux density for a four poles surface mounted PMSM, where one magnet is smaller (solid) and for the ideal machine (dotted). A schematic of the rotor is shown below the course of the function.

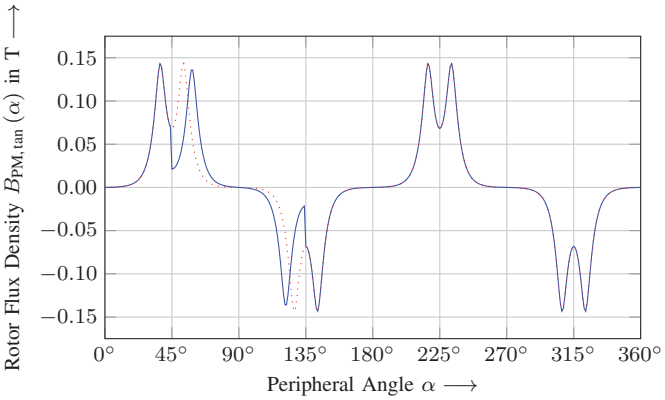

Fig. 6. Tangential rotor flux density for a four poles surface mounted PMSM, where one magnet is smaller (solid) and for the ideal machine (dotted).

Neumann boundary condition at the inner stator radius, which represents an unslotted stator with infinite high permeability. The resulting flux density distribution is sampled in the middle of the original air gap. A comparison is shown in Fig. 7 for the radial rotor flux density and in Fig. 8 for the tangential one. The previously presented flux densities, calculated with help of the CM approach, are drawn solid. The FE simulated functions are plotted with dots. The entire course of the functions is in good agreement. The transitions between two pole pitches are slightly smoother if calculated with FE.

As shown for the permeance function, the influence of eccentricity has to be considered for the rotor flux density as well. Comparable to (10) and (11), the rotor flux density is weighted by a sinusoid. With help of the conformal mapping approach, the rotor flux density is calculated once for the smallest air gap δ_{min} and once for the largest air gap δ_{max}. Then the eccentricity afflicted rotor flux density $\underline{B}_{\mathrm{PM,\,ecc}}\left(\alpha, t\right)$ is computed sinusoidal between the rotor flux densities for the smallest and largest air gap:

$$\underline{B}_{\mathrm{PM,\,ecc}}\left(\alpha, t\right) = \underline{B}_{\mathrm{PM}}\left(\alpha, t\right) + \frac{\underline{B}_{\mathrm{PM,\,min}} - \underline{B}_{\mathrm{PM,\,max}}}{\delta_{\mathrm{max}} - \delta_{\mathrm{min}}} \cdot e \cdot \cos\left(\alpha - \omega - \varphi\right) , \qquad (14)$$

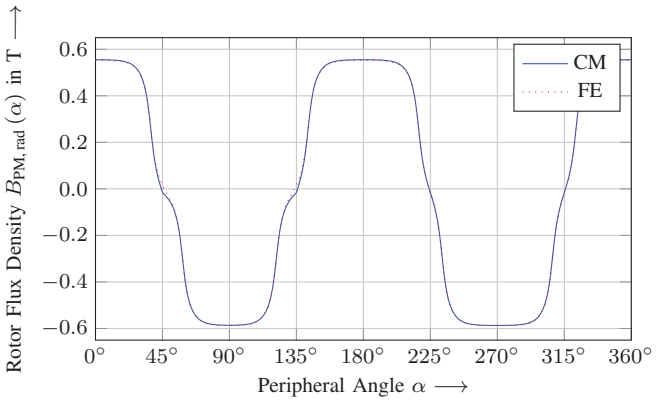

Fig. 7. Radial rotor flux density for a four poles surface mounted PMSM, where one magnet is smaller, calculated with CM and with FE.

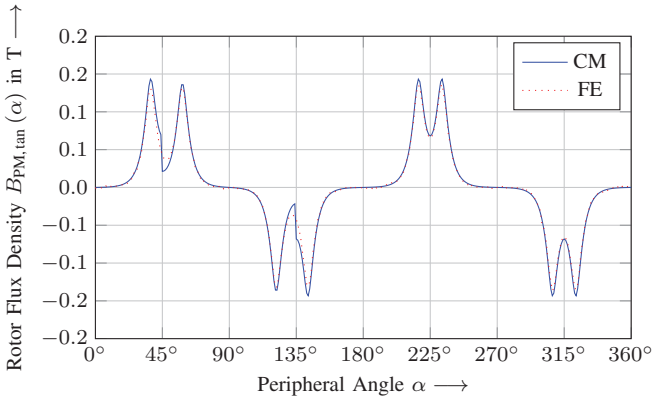

Fig. 8. Tangential rotor flux density for a four poles surface mounted PMSM, where one magnet is smaller, calculated with CM and with FE.

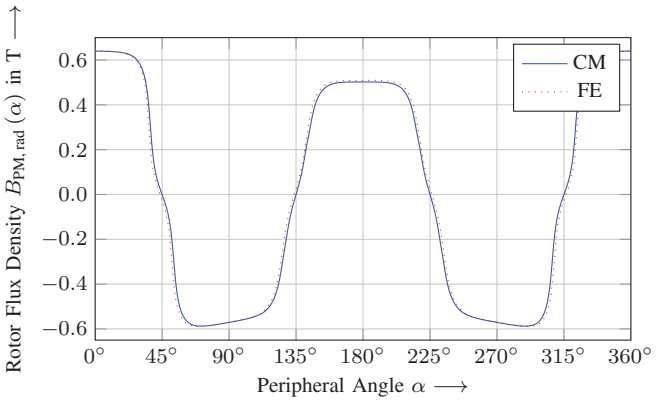

Fig. 9. Radial rotor flux density for a four poles surface mounted PMSM with a static eccentricity of 0.5 mm calculated with CM and with FE.

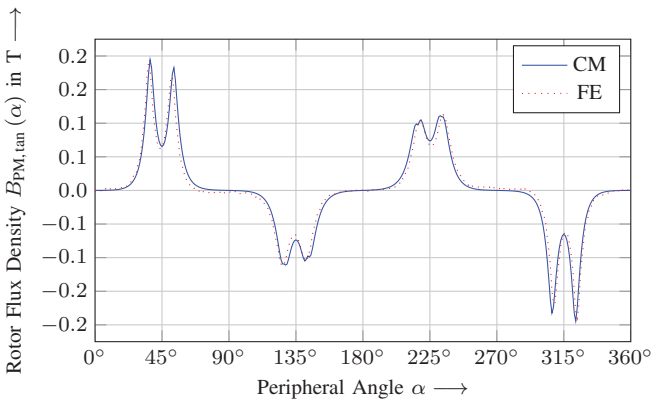

Fig. 10. Tangential rotor flux density for a four poles surface mounted PMSM with a static eccentricity of 0.5 mm calculated with CM and with FE.

where $\underline{B}_{\mathrm{PM,max}}$ is the rotor flux density in radial and tangential direction for the largest air gap and $\underline{B}_{\mathrm{PM,min}}$ the rotor flux density for the smallest air gap.

Results of the analytical calculation with a static eccentricity of 0.5 mm and a comparison to the results determined by FE are shown in Fig. 9 for the radial rotor flux density and in Fig. 10 for the tangential one. They are in good agreement.

C. Stator Flux Density

The stator's magnetic air gap field is created by the current conducting coils. In [3] is described, that the magnetic field distribution due to a current of one ampere in a single slot, assuming an infinite slot depth and an infinite permeability in an otherwise slotless stator, can be obtained by conformal mapping. For the ideal machine without manufacturing tolerances, this field distribution is calculated just once and is then assembled to the stator flux density in dependence of the winding scheme and the phase currents.

In order to model the influence of manufacturing deviations on the stator flux density, this current field distribution has to be calculated with the CM approach for every different slot geometry, which is similar to the calculation of the tolerance afflicted stator permeance function. The field distribution is then determined for every coil of the winding scheme. One coil consists of a forward conductor and a corresponding backward conductor. The slots which do not belong to the coil are connected linear. Fig. 11a shows the flux density distribution for the second coil, which is winded around the second tooth. Again, the third tooth is displaced, so that the course of the function for the second slot pitch (60°–128°) is slightly different than the negative course for the third slot pitch (128°–180°). In the next step, the linear connections are weighted with the permeance function from Fig. 1 which results in Fig. 11b. In order to take an eccentricity into account, the whole function is first divided by the permeance function $\underline{\lambda}(\alpha)$, where the eccentricity is not considered:

$$\underline{B}_{\mathrm{Stator,\,w/o\,\lambda}}(\alpha) = \underline{B}_{\mathrm{Stator,\,\lambda}}(\alpha) / \underline{\lambda}^{*}(\alpha) \,, \tag{15}$$

which yields the permeance free stator flux density distribution $\underline{B}_{\mathrm{Stator,\,w/o\,\lambda}}(\alpha)$ for one coil. This result is revealed in Fig. 11c. The last steps are the multiplication with the eccentricity afflicted permeance function $\underline{\lambda}_{\mathrm{ecc}}(\alpha, t)$ and the adjustment by a correction term for every time step, to obtain a divergence free flux density for the stator. The final stator flux density distribution, where the tooth displacement and the eccentricity are considered, is shown in Fig. 11d. The influence of eccentricity is difficult to see in this figure. Now, this function can be weighted by the coil's number of turns and

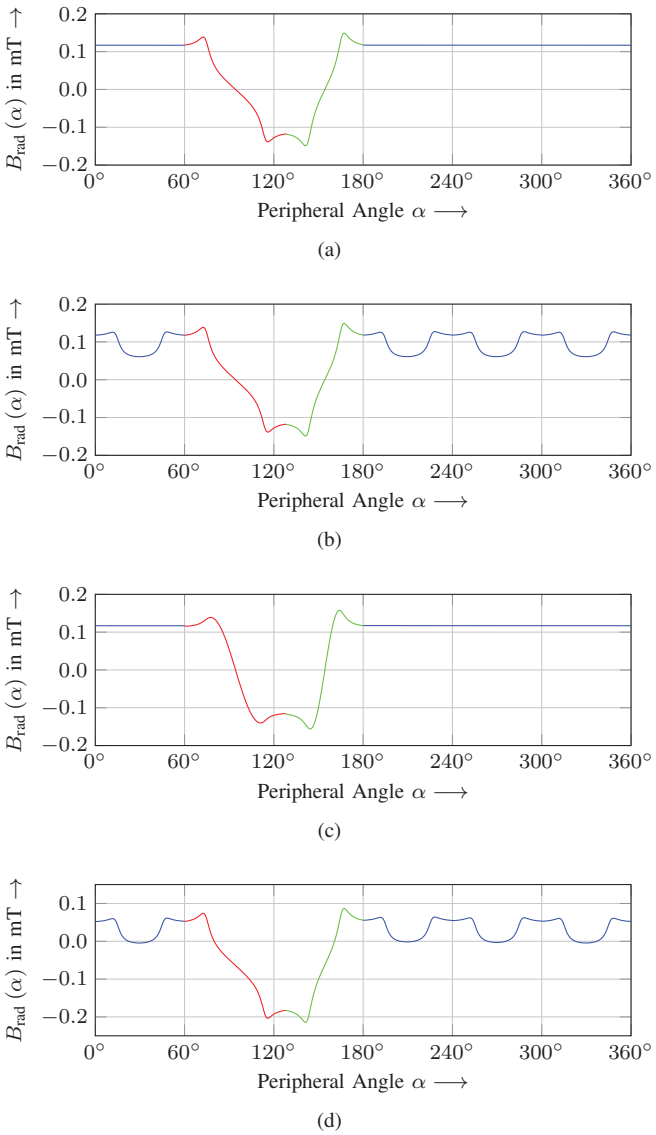

Fig. 11. Building of the radial stator flux density for the second coil of a six teeth and four poles surface mounted PMSM, where the third tooth is displaced and with a static eccentricity of 0.5 mm.

the current in the coil for every time step. Consequently, coil manufacturing tolerances, like different numbers of turns per coil, can be considered in this step as well.

D. Air Gap Flux Density

Now, the manufacturing tolerances are considered in all of the three contributing air gap field components. The resulting magnetic air gap field $\underline{B}_{\text{Airgap}}(\alpha, t)$ for the electrical machine with tolerances is calculated with the help of (1) for every time step. In Fig. 12, the resulting radial air gap field for the surface mounted PMSM is presented in solid. The machine has an exemplarily dynamic eccentricity of 0.5 mm and is operating with the rated current of 2.3 A. Shown is the resulting magnetic air gap field for the first time step of the simulation.

A FE simulation is performed again in order to validate the CM approach. The conditions chosen are the same as for the CM approach and are presented in Table I. The resulting flux

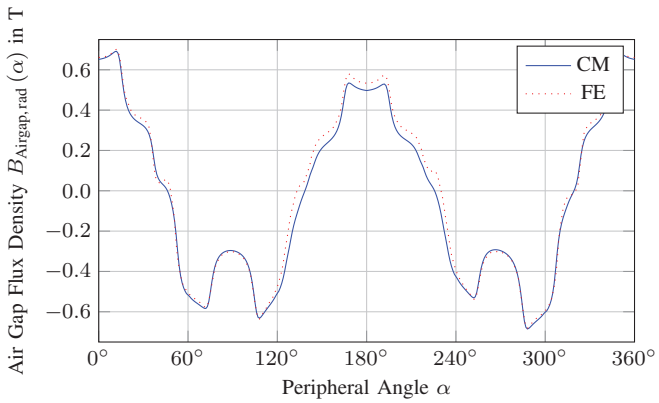

Fig. 12. Radial air gap flux density for a six teeth and four poles surface mounted PMSM operating with the rated current of 2.3 A and a dynamic eccentricity of 0.5 mm. Shown is the first time step.

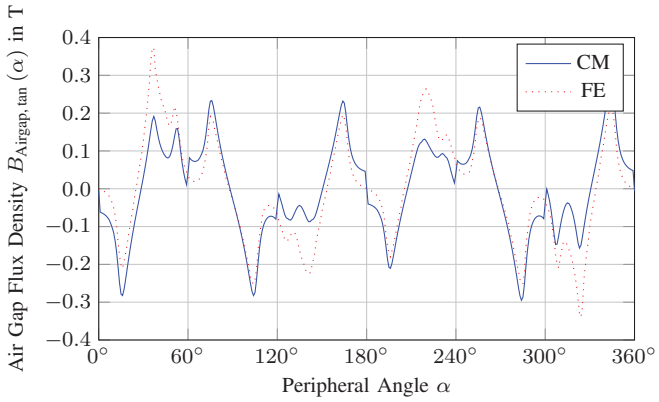

Fig. 13. Tangential air gap flux density for a six teeth and four poles surface mounted PMSM operating with the rated current of 2.3 A and a dynamic eccentricity of 0.5 mm. Shown is the first time step.

density distribution is sampled in the middle of the air gap. A comparison is shown in Fig. 12. The function determined by FE is drawn dotted. The overall courses of both functions are in good agreement. They differ slightly for the largest air gap in the region around 180°. There, the CM approach yields smaller values than the FE simulation.

Fig. 13 shows the corresponding resulting tangential air gap field and the comparison between the analytical CM approach and the FE simulation. The difference between the two courses is apparently greater. Especially in the regions around 40°, 140°, 220° and 320° the results determined by FE are larger.

III. Manufacturing Tolerances Influence on Radial Force Densities

After the whole magnetic air gap field is determined, the radial force density is calculated by means of (4). This results in a matrix which contains the radial force density $\sigma_{\text{rad}}(\alpha, t)$ for every discrete point in space and time. A 2-D discrete Fourier transformation yields the force density magnitudes $\hat{\sigma}_{\text{rad}}(\nu, \mu)$ over spatial and frequency order, as described in [10].

Fig. 14 shows the so computed force density magnitudes $\hat{\sigma}_{\text{rad}}$ for the six teeth and four poles surface mounted PMSM without manufacturing tolerances as a function of spatial

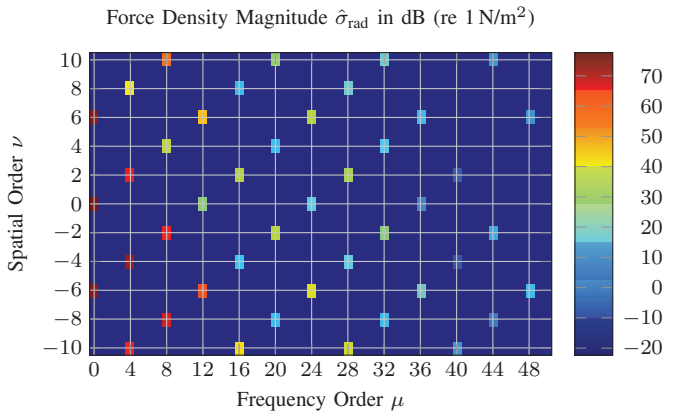

Fig. 14. Radial force density magnitudes for a six teeth and four poles surface mounted PMSM without manufacturing tolerances as a function of spatial order ν and frequency order μ.

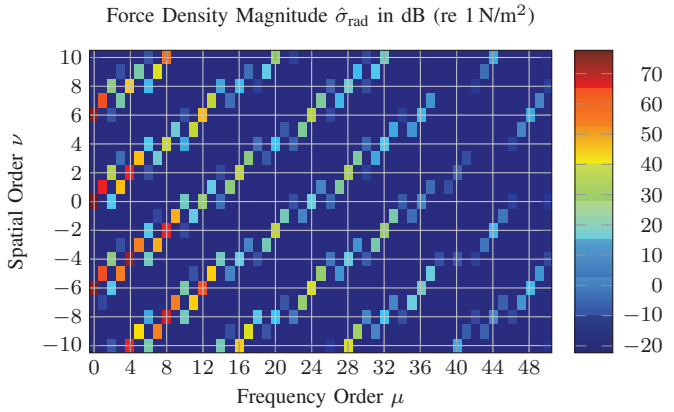

Fig. 15. Radial force density magnitudes for a six teeth and four poles surface mounted PMSM with a dynamic eccentricity of 0.5 mm as a function of spatial order ν and frequency order μ.

order ν and frequency order μ. The height of the magnitudes is represented by different colors. E. g. dark red stands for a height of over 70 dB with reference to 1 N/m^2. This is equivalent to approximately 7500 N/m^2. The magnitude of every fourth frequency order is distinctive, because of the machine's four poles. The same behavior can be seen for the spatial order, where every sixth order dominates, which matches with the number of stator teeth.

The same calculation is performed for the machine with a dynamic rotor eccentricity of 0.5 mm. The resulting force density magnitudes are presented in Fig. 15. Around the main orders from Fig. 14, additional orders with a minor amplitude occur at ± 1 of the spatial and frequency order, because of the dynamic rotor eccentricity. These so computed orders match with the orders calculated by analytical considerations [9], but with the benefit that the magnitudes of the additional orders can be estimated as well.

The effect of static tolerances, like static eccentricity or deviations in the teeth' geometry, compared to dynamic deviations, like dynamic eccentricity or magnet tolerances, where the error rotates with rotor speed, can clearly be distinguished in the spectra. Whereas static tolerances just excite new force densities with the same spatial orders as the ideal symmetric machine, dynamic tolerances arouse new frequency orders in addition, as shown in Fig. 15. Sum forces, like the torque (7) or the unbalanced magnetic pull (8) can be derived and analyzed from the force densities as well.

IV. Conclusion

This paper addressed the analytical modeling of manufacturing tolerances for surface mounted PMSMs with the help of the conformal mapping approach. The modeling of different manufacturing tolerances was described and the tolerances' influence on the relative permeance function, the magnetic air gap field of the rotor and the stator's magnetic air gap field was shown. The analytical calculated rotor's air gap field as well as the whole resulting air gap field for different tolerance cases were compared to results determined by means of finite element simulations and are in good agreement. Results for the radial flux density component are more accurate than for the tangential component.

The force density magnitudes for a machine without manufacturing tolerances and with a dynamic rotor eccentricity were exhibited as a result computed with the presented approach. The orders match with the orders calculated by analytical considerations, but with the benefit that the magnitudes of the orders can be estimated as well. So the impact on radial force densities can be calculated and compared within seconds for different machine topologies and different manufacturing tolerances, whereas FE simulations need at least one full electrical period of calculations.

References

[1] F. W. Carter, "The magnetic field of the dynamo-electric machine", *Journal of the Institution of Electrical Engineers*, Vol. 64, No. 359, pp. 1115–1138, Nov. 1926.

[2] D. Žarko, D. Ban, and T. A. Lipo, "Analytical Calculation of Magnetic Field Distribution in the Slotted Air Gap of a Surface Permanent-Magnet Motor Using Complex Relative Air-Gap Permeance", *IEEE Transactions on Magnetics*, Vol. 42, No. 7, pp. 1828–1837, Jul. 2006.

[3] M. Hafner, D. Franck, and K. Hameyer, "Static Electromagnetic Field Computation by Conformal Mapping in Permanent Magnet Synchronous Machines", *IEEE Transactions on Magnetics*, Vol. 46, No. 8, pp. 3105–3108, Aug. 2010.

[4] L. J. Wu, Z. Q. Zhu, J. T. Chen, and Z. P. Xia, "An Analytical Model of Unbalanced Magnetic Force in Fractional-Slot Surface-Mounted Permanent Magnet Machines", *IEEE Transactions on Magnetics*, Vol. 46, No. 7, pp. 2686–2700, Jul. 2010.

[5] A. Ruf, M. Schröder, A. K. Putri, D. Franck, and K. Hameyer, "Analysis and determination of mechanical bearing load caused by unbalanced magnetic pull", *17th International Conference on Electrical Machines and Systems*, pp. 8–14, Oct. 2014.

[6] R. C. Robinson, "The calculation of unbalanced magnetic pull in synchronous and induction motors", *Electrical Engineering*, Vol. 62, No. 10, pp. 620–623, Oct. 1943.

[7] W. Zhu, B. Fahimi, and S. Pekarek, "A Field Reconstruction Method for Optimal Excitation of Permanent Magnet Synchronous Machines", *IEEE Transactions on Energy Conversion*, Vol. 21, No. 2, pp. 305–313, Jun. 2006.

[8] M. Hafner, D. Franck, and K. Hameyer, "Conformal mapping approach for permanent magnet synchronous machines: on the modeling of saturation", *Archives of Electrical Engineering*, Vol. 61, No. 2, pp. 211–220, Jun. 2012.

[9] J. F. Gieras, C. Wang, and J. Cho Lai, *Noise of Polyphase Electric Motors*, CRC Press (Taylor & Francis Group), USA, 2006.

[10] M. Schröder, D. Franck, and K. Hameyer, "Evaluation of magnitude- and phase-correct unit-force transfer functions for the structural description of electrical machines", *International Journal of Applied Electromagnetics and Mechanics*, Vol. 46, No. 2, pp. 401–407, Jun. 2014.